A Low-complexity Channel Shortening Receiver with Diversity Support for Evolved 2G Devices

Sha Hu[†], Harald Kröll[‡], Qiuting Huang[‡], and Fredrik Rusek[†]
[†]Department of Electrical and Information Technology, Lund University, Lund, Sweden
[‡]Integrated Systems Laboratory, ETH Zürich, Switzerland
[†]{sha.hu, fredrik.rusek}@eit.lth.se, [‡]{kroell, huang}@iis.ee.ethz.ch

arXiv:1511.07702v1 [cs.IT] 24 Nov 2015

***Abstract*—The second generation (2G) cellular networks are the current workhorse for machine-to-machine (M2M) communications. Diversity in 2G devices can be present both in form of multiple receive branches and blind repetitions. In presence of diversity, intersymbol interference (ISI) equalization and co-channel interference (CCI) suppression are usually very complex. In this paper, we consider the improvements for 2G devices with receive diversity. We derive a low-complexity receiver based on a channel shortening filter, which allows to sum up all diversity branches to a single stream after filtering while keeping the full diversity gain. The summed up stream is subsequently processed by a single stream Max-log-MAP (MLM) equalizer. The channel shortening filter is designed to maximize the mutual information lower bound (MILB) with the Ungerboeck detection model. Its filter coefficients can be obtained mainly by means of discrete-Fourier transforms (DFTs). Compared with the state-of-art homomorphic (HOM) filtering based channel shortener which cooperates with a delayed-decision feedback MLM (DDF-MLM) equalizer, the proposed MILB channel shortener has superior performance. Moreover, the equalization complexity, in terms of real-valued multiplications, is decreased by a factor that equals the number of diversity branches.**

I. Introduction

Although in some parts of the world 2G networks are replaced by cutting-edge 4G and beyond networks, nowadays 2G networks are the workhorse for emerging M2M communications [1], longevity of 2G networks is predicted not least only since it offers global ubiquitous coverage and has the largest number of subscribers worldwide.

In order to make 2G networks competitive with other standards which intend to conquer the 200kHz bands, several extensions have been proposed over time. Some extensions aim for better coverage while others aim for higher throughput and better robustness against interference. What many extensions have in common is the use of diversity. For example, in extended coverage GSM (EC-GSM), coverage is improved to reach, e.g., deep-indoor devices via blind repetition diversity [2]. Hereby the same GSM radio burst is transmitted repeatedly to ease reception by the IoT device. Another extension called Evolved EDGE (E-EDGE) [3] aims at improving the fallback capability of 2G networks, and to make user experience less frustrating when loosing broadband connectivity of e.g. 4G cellular networks. To provide a reliable fallback solution, E-EDGE offers up to 1Mbit/s downlink data rate. Moreover, antenna diversity is used to increase throughput under noisy and interference prone environments. This is especially attractive for 4G-enabled smart phones, where more that two receive antennas are specified.

Despite all the advantages that diversity offers regarding coverage extension and interference robustness, it makes signal processing in the receiver very complex, especially since single carrier 2G systems suffer from ISI and CCI, whereas the adjacent-channel interference can be mitigated through low-pass filters. To suppress CCI, the space-time filter (STF) is proposed in [4]. It is a joint filtering and channel estimation algorithm that combines the multiple received streams into a single stream and maximizes the signal to interference and noise ratio. However, as shown in [4], the ISI should not be handled by the STF since it causes noise enhancement. Furthermore, after STF the ISI duration is prolonged, which increases the complexity for ISI equalization. On the other hand, due to the limited length of the training symbols, a joint optimization of the STF over multiple branches is infeasible. This is due to the fact that, the correlation matrix of the received samples corresponding to the training symbols becomes singular as the number of diversity branches increases.

Therefore, in this paper we propose a low-complexity receiver for ISI channels with multiple diversity branches, which is able to achieve the full diversity gain with a single stream equalizer. It contains two stages: (1) interference suppression to suppress the CCI, and (2) channel shortener to reduce the number of states in ISI equalization. Different from STF, in the first stage we suppress the interference based on the least square (LS) criteria and keep the ISI channel of the target user unchanged. Besides interference suppression, the receiver needs to deal with the ISI introduced by the frequency-selective channels.

The MLM equalizer [5] implements the maximum log-likelihood sequence estimation [6] with soft decisions. However, the number of states in the equalizer increases exponentially with the ISI duration. Therefore, techniques of channel shortening were developed to reduce the number of the states in the equalizer by filtering the ISI channel with a prefilter. Traditionally, the minimal phase filter [7] is utilized to concentrate the energy of the channel impulse response (CIR) to the first few taps. Efficient design of the prefiters based on homomorphic filtering can be found in [8], [9]. The signal parts corresponding to the channel tails with smaller energy are removed from the received signal by the delayed-decision feedbacks [10] and results in the DDF-MLM equalizer.

In [11], the authors proposed a different design of the channel shortener and the MLM equalizer is based on the Ungerboeck model [12]. The channel shortener is designed to maximize the lower bound of the information rate corresponding to a mismatched detection model. We call this approach the MILB demodulator, which contains a MILB channel shortener and MLM equalizer with channel tails truncated. The MILB demodulator was successfully applied to E-EDGE system in [13]. However, [11] and [13] solely deal with a single receive antenna ISI channel.

In this paper, we extend the MILB demodulator to support diversity which combines multiple diversity branches into a single data stream. As shown in Section IV, the proposed two-stage receiver is efficient in suppressing the CCI. Furthermore, with significantly reduced complexity in the equalizer, the MILB demodulator has a superior performance than the homomorphic filtering based channel shortener followed by the DDF-MLM equalizer. We denote the latter approach as the HOM demodulator.

Notations:

Throughout the paper, $\boldsymbol{I}$ represents an identity matrix, superscripts "$^{\mathrm{T}}$" and "†" denote the matrix transpose and Hermitian transpose, respectively. In addition, "$\mathrm{Tr}(\,)$" is the trace operator, "$\mathcal{R}\{\,\}$" fetches the real part of a variable, "$*$" denotes the linear convolution, and "$\otimes$" is the tensor product.

II. Single-Input Multi-Output Signal Model

Consider a single-input and multi-output (SIMO) system with N diversity branches and M interferers. The symbols are transmitted over frequency-selective channels with additive white noise. The received sample y_k^n on the nth diversity branch can be modeled as

$$y_k^n = \sum_{\ell=0}^{L-1} h_\ell^n x_{k-\ell} + \sum_{m=0}^{M-1}\sum_{\ell=0}^{\tilde{L}-1} p_\ell^{n,m} s_{k-\ell}^m + n_k^n, \tag{1}$$

where x_k is the transmit signal of the target user, s_k^m is the transmit signal from the mth interferer, and n_k^n is the noise variable on the nth receive branch, all at time k. The ℓth tap of the CIR on the nth diversity branch corresponding to the target user and the mth interferer are denoted as h_ℓ^n and $p_\ell^{m,n}$, respectively. The longest ISI duration over all branches of the target user and interferers are denoted as L and $\tilde{L}$, respectively. We assume that the noise variables n_k^n are zero-mean complex Gaussian random variables with variance N_0.

Let z_k^n denote the interference term on the nth branch as

$$z_k^n = \sum_{m=0}^{M-1}\sum_{\ell=0}^{\tilde{L}-1} p_\ell^{n,m} s_{k-\ell}^m + n_k^n,$$

then model (1) can be written as

$$y_k^n = \sum_{\ell=0}^{L-1} h_\ell^n x_{k-\ell} + z_k^n. \tag{2}$$

Let $\boldsymbol{y}_k = [y_k^0\ y_k^1\ \ldots\ y_k^{N-1}]^{\mathrm{T}}$ and $\boldsymbol{z}_k = [z_k^0\ z_k^1\ \ldots\ z_k^{N-1}]^{\mathrm{T}}$ be the vectors that comprise the received samples and interference from all N diversity branches, respectively. Then model (2) can be written in the vector form

$$\boldsymbol{y}_k = \sum_{\ell=0}^{L-1} \boldsymbol{h}_\ell x_{k-\ell} + \boldsymbol{z}_k, \tag{3}$$

where the $N\times 1$ vector $\boldsymbol{h}_\ell$ comprising the ℓth tap CIR from all diversity branches reads

$$\boldsymbol{h}_\ell = [h_\ell^0\ h_\ell^1\ \ldots\ h_\ell^N]^{\mathrm{T}}. \tag{4}$$

Further, define the $NK\times 1$ vectors $\boldsymbol{y}_{k:K}$ and $\boldsymbol{z}_{k:K}$, and the $(K+L-1)\times 1$ vector $\boldsymbol{x}_k$ as

$$\begin{aligned}
\boldsymbol{y}_{k:K} &= [\boldsymbol{y}_k^{\mathrm{T}}\ \boldsymbol{y}_{k+1}^{\mathrm{T}}\ \cdots\ \boldsymbol{y}_{k+K-1}^{\mathrm{T}}]^{\mathrm{T}},\\
\boldsymbol{z}_{k:K} &= [\boldsymbol{z}_k^{\mathrm{T}}\ \boldsymbol{z}_{k+1}^{\mathrm{T}}\ \cdots\ \boldsymbol{z}_{k+K-1}^{\mathrm{T}}]^{\mathrm{T}},\\
\boldsymbol{x}_{k:K} &= [x_{k-L+1}\ x_{k-L+2}\ \cdots\ x_{k+K-1}]^{\mathrm{T}}.
\end{aligned} \tag{5}$$

Then the signal model (3) that comprises a total of NK received scalar samples reads

$$\boldsymbol{y}_{k:K} = \boldsymbol{H}\boldsymbol{x}_{k:K} + \boldsymbol{z}_{k:K}, \tag{6}$$

and the $NK\times(K+L-1)$ convolution matrix $\boldsymbol{H}$ is

$$\boldsymbol{H} = \begin{bmatrix}
\boldsymbol{h}_{L-1} & \cdots & \boldsymbol{h}_1 & \boldsymbol{h}_0 & & \\
 & \boldsymbol{h}_{L-1} & \ddots & \boldsymbol{h}_1 & \boldsymbol{h}_0 & \\
 & & \ddots & \ddots & \ddots & \ddots \\
 & & & \boldsymbol{h}_{L-1} & \cdots & \boldsymbol{h}_1\ \boldsymbol{h}_0
\end{bmatrix}.$$

Based on signal models (3) and (6), in Section II-A below we lay down the channel estimation module that will be used in both stages of the receiver. In Section II-B we discuss the noise estimation that will be used in the second stage.

A. Least Square Channel Estimation

In an E-EDGE alike system, the CIR of the target user can be estimated through training symbols. Assume that $\boldsymbol{x}_{k_0:K_0}$ are the transmitted training symbols with length $\nu = K_0 + L - 1$ as defined in (5). From (6), it holds that

$$\boldsymbol{y}_{k_0:K_0} = \boldsymbol{H}\boldsymbol{x}_{k_0:K_0} + \boldsymbol{z}_{k_0:K_0}. \tag{7}$$

Firstly, we define a useful operator $\mathcal{T}(\boldsymbol{a}, L)$ that generates a $(K-L+1)\times L$ matrix by cyclically shifting the elements of the $K\times 1$ vector $\boldsymbol{a} = [a_0\ a_1\ \ldots\ a_{K-1}]^{\mathrm{T}}$ as below:

$$\mathcal{T}(\boldsymbol{a}, L) = \begin{bmatrix}
a_{L-1} & a_{L-2} & \cdots & a_0 \\
a_L & a_{L-1} & \cdots & a_1 \\
\vdots & \vdots & \vdots & \vdots \\
a_{K-1} & a_{K-2} & \cdots & a_{K-L}
\end{bmatrix}. \tag{8}$$

Define the $K_0\times L$ matrix $\boldsymbol{S} = \mathcal{T}(\boldsymbol{x}_{k_0:K_0}, L)$ which is generated from the $\nu\times 1$ training symbol vector $\boldsymbol{x}_{k_0:K_0}$. Further, let the vectors $\boldsymbol{y}_{k_0:K_0}^n$ and $\boldsymbol{z}_{k_0:K_0}^n$ comprise the the received samples and interference terms from time k_0 to k_0+K_0-1 on the nth diversity branch, respectively, which are defined as

$$\begin{aligned}
\boldsymbol{y}_{k_0:K_0}^n &= [y_{k_0}^n\ y_{k_0+1}^n\ \cdots\ y_{k_0+K_0-1}^n]^{\mathrm{T}},\\
\boldsymbol{z}_{k_0:K_0}^n &= [z_{k_0}^n\ z_{k_0+1}^n\ \cdots\ z_{k_0+K_0-1}^n]^{\mathrm{T}}.
\end{aligned} \tag{9}$$

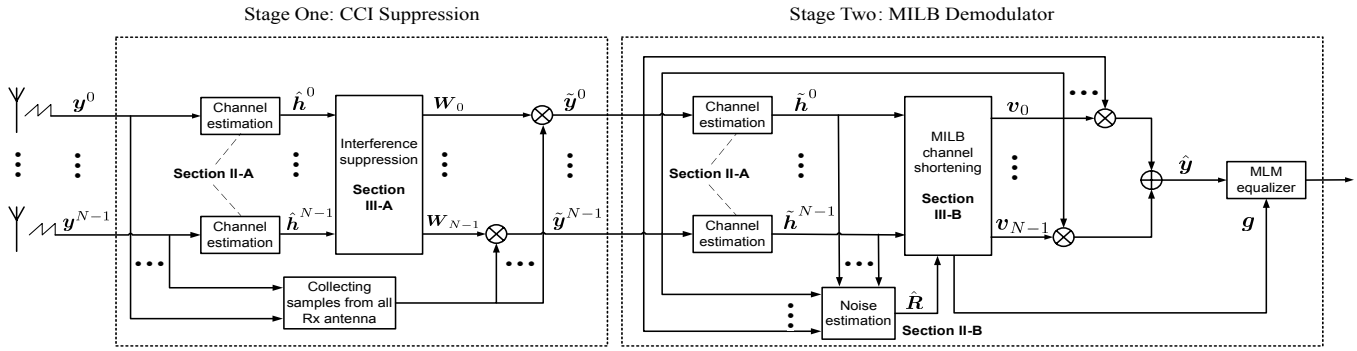

Fig. 1. The two-stage receiver with CCI suppression and the MILB demodulator. The branches $\boldsymbol{y}^0$ to $\boldsymbol{y}^{N-1}$ can alternatively be obtained from different blind repetitions in the repetition diversity [2].

Then from model (7), we have

$$\boldsymbol{y}^n_{k_0:K_0} = \boldsymbol{S}\boldsymbol{h}^n + \boldsymbol{z}^n_{k_0:K_0}, \tag{10}$$

where the $L \times 1$ vector $\boldsymbol{h}^n$ comprising the CIR on the nth diversity branch reads

$$\boldsymbol{h}^n = [h^n_0 \; h^n_1 \; \cdots \; h^n_{L-1}]^{\mathrm{T}}.$$

Therefore, the LS channel estimate of $\boldsymbol{h}^n$, which is denoted as $\hat{\boldsymbol{h}}^n$, can be obtained through

$$\hat{\boldsymbol{h}}^n = \left(\boldsymbol{S}^\dagger \boldsymbol{S}\right)^{-1} \boldsymbol{S}^\dagger \boldsymbol{y}^n_{k_0:K_0}. \tag{11}$$

B. Noise Estimation

Based on the channel estimates in (11), the estimate of $\boldsymbol{h}_\ell$ in (4) can be obtained, which we denote as $\hat{\boldsymbol{h}}_\ell$. From model (3), the $N \times N$ covariance matrix $\boldsymbol{R}$ which represents the spatial correlation of the interference is estimated through

$$\begin{aligned}\hat{\boldsymbol{R}} &= \mathbb{E}\left[\hat{\boldsymbol{z}}_k \hat{\boldsymbol{z}}_k^\dagger\right] \\ &= \frac{1}{K_0} \sum_{k=k_0}^{k_0+K_0-1} \hat{\boldsymbol{z}}_k \hat{\boldsymbol{z}}_k^\dagger,\end{aligned} \tag{12}$$

where

$$\hat{\boldsymbol{z}}_k = \boldsymbol{y}_k - \sum_{\ell=0}^{L-1} \hat{\boldsymbol{h}}_\ell x_{k-\ell}.$$

Since the CCI is effectively suppressed by the interference suppression process on each diversity branch at the first stage, the temporary correlation of the interference is not further considered at the second stage in the receiver.

III. The Structure of the Two-Stage Receiver

In Section II, we have discussed the channel and noise estimates based on the training symbols. In this section, we elaborate on the structure of the two-stage receiver as depicted in Figure 1. At the first stage, the samples are filtered by a group of filters $\boldsymbol{W}_n$ to suppress the CCI. The filtering is applied to mitigate interference without dealing with the ISI channel of the target user. Then at the second stage, based on the filtered samples $\tilde{\boldsymbol{y}}$, the channel estimate $\tilde{\boldsymbol{H}}$ and noise covariance matrix $\hat{\boldsymbol{R}}$ are updated and sent to the MILB channel shortening module, which generates the prefilters $\boldsymbol{v}_n$ and the coefficient $\boldsymbol{g}$ that will be used in the MLM equalizer. Samples on different branches are filtered and then summed up to a single data stream $\hat{\boldsymbol{y}}$. Unlike DDF-MLM equalizer in the HOM demodulator which needs parallel branch metric computation for each diversity branch, the MLM equalizer in the MILB demodulator only requires a single branch metric calculation. The complexity of the HOM and MILB demodulators will be further discussed in Section III-C.

A. Stage One: CCI Suppression

At the first stage, the received samples $\boldsymbol{y}^m$ are filtered by the filters $\boldsymbol{w}_{n,m}$ $(0 \le n, m < N)$ to suppress the CCI. The filters have tap length L_w (a design parameter) and are designed based on the signal model (10) to minimize the estimation error on the mth branch, which is

$$\boldsymbol{e}_n = \min_{\boldsymbol{w}_{n,m}} \left| \sum_{m=0}^{N-1} \boldsymbol{w}_{n,m} * \boldsymbol{y}^m_{k_0:K_0} - \hat{\boldsymbol{h}}^n * \boldsymbol{x}_{k_0:K_0-L_w+1} \right|^2.$$

The error $\boldsymbol{e}_n$ can be written in the matrix form as

$$\begin{aligned}\boldsymbol{e}_n &= \min_{\boldsymbol{w}_{n,m}} \left| \sum_{m=0}^{N-1} \boldsymbol{T}_2^m \boldsymbol{w}_{n,m} - \boldsymbol{T}_3 \hat{\boldsymbol{h}}^n \right|^2 \\ &= \min_{\boldsymbol{W}_n} \left| \boldsymbol{\zeta}_2 \boldsymbol{W}_n - \boldsymbol{T}_3 \hat{\boldsymbol{h}}^n \right|^2,\end{aligned} \tag{13}$$

where

$$\boldsymbol{\zeta}_2 = \left[\boldsymbol{T}_2^0 \; \boldsymbol{T}_2^1 \; \cdots \; \boldsymbol{T}_2^{N-1}\right],$$

and

$$\boldsymbol{W}_n = \left[\boldsymbol{w}_{n,0}^{\mathrm{T}} \; \boldsymbol{w}_{n,1}^{\mathrm{T}} \; \cdots \; \boldsymbol{w}_{n,N-1}^{\mathrm{T}}\right]^{\mathrm{T}}.$$

The $(K_0 - L_w + 1) \times L_w$ matrix $\boldsymbol{T}_2^m$ and $(K_0 - L_w + 1) \times L$ matrix $\boldsymbol{T}_3$ are generated by the operator $\mathcal{T}$ specified in (8):

$$\begin{aligned}\boldsymbol{T}_2^m &= \mathcal{T}(\boldsymbol{y}^m_{k_0:K_0}, L_w), \\ \boldsymbol{T}_3 &= \mathcal{T}(\boldsymbol{x}_{k_0:K_0-L_w+1}, L),\end{aligned}$$

where $\boldsymbol{y}^m_{k_0:K_0}$ and $\boldsymbol{x}_{k_0:K_0-L_w+1}$ are the vectors comprising of received samples on the mth diversity branch and the training

symbols as in (9) and (5), respectively. The estimate $\hat{\boldsymbol{h}}^n$ on the nth branch has been obtained through (11). Taking the first order differential of $\boldsymbol{W}_n$ in (13) yields the optimal filter

$$\boldsymbol{W}_n = \boldsymbol{\zeta}_2^\dagger \left(\boldsymbol{\zeta}_2 \boldsymbol{\zeta}_2^\dagger\right)^{-1} \boldsymbol{T}_3 \hat{\boldsymbol{h}}^n.$$

The received samples $\boldsymbol{y}^m$ are then filtered by the filters $\boldsymbol{w}_{n,m}$ to obtain the purified data on nth diversity branch as

$$\tilde{\boldsymbol{y}}_n = \sum_{m=0}^{N-1} \boldsymbol{w}_{n,m} \boldsymbol{y}^m.$$

After filtering, the signal model (6) still holds for a data transmit block with size $K+L-1$ as

$$\tilde{\boldsymbol{y}}_{k:K} = \boldsymbol{H}\boldsymbol{x}_{k:K} + \tilde{\boldsymbol{z}}_{k:K}, \tag{14}$$

where $\tilde{\boldsymbol{z}}_k$ is the residual interference after the CCI suppression. Furthermore, updated channel and noise estimates are obtained through (11) and (12) with filtered samples $\tilde{\boldsymbol{y}}_n$ in (14), which will be sent into the MILB channel shortening module in the second stage of the receiver.

B. Stage Two: MILB Channel Shortening Algorithm

The MILB channel shortener extends the framework developed in [11] to deal with multiple diversity branches. With ISI channels, the MILB channel shortening is developed when the block size $K+L-1$ is infinite, in which case, we can let the channel matrix $\boldsymbol{H}$ represent circular convolution instead of the linear convolution with a L-tap ISI channel on each diversity branch. This approximation[1] can reach any given precision [14] and is a result of Szegö's eigenvalue distribution theorem [15]. With such assumption, we can rewrite the model (14) as,

$$\boldsymbol{Y} = \boldsymbol{H}\boldsymbol{X} + \boldsymbol{Z}, \tag{15}$$

where $\boldsymbol{Y}$ and $\boldsymbol{X}$ are $K \times 1$ vectors representing the received samples and transmit signal, respectively. The vector $\boldsymbol{Z}$ is a complex Gaussian noise vector that obeys $\boldsymbol{Z} \sim \mathrm{CN}(\boldsymbol{0}, \boldsymbol{I} \otimes \boldsymbol{R})$. The $NK \times K$ block circulant matrix $\boldsymbol{H}$ is generated by its first column $[\boldsymbol{h}_0 \ \boldsymbol{h}_1 \ \cdots \ \boldsymbol{h}_{L-1} \ \boldsymbol{0} \ \cdots \ \boldsymbol{0}]^{\mathrm{T}}$. Assuming that the demodulator operates on the Ungerboeck model $T(\boldsymbol{Y}|\boldsymbol{X})$, which is

$$T(\boldsymbol{Y}|\boldsymbol{X}) = \exp\left(-2\mathcal{R}\left\{\boldsymbol{X}^\dagger \boldsymbol{V}^\dagger \boldsymbol{Y}\right\} + \boldsymbol{X}^\dagger \boldsymbol{G} \boldsymbol{X}\right), \tag{16}$$

the lower bound of the information rate is defined as

$$I_{\mathrm{R}} = -\mathfrak{h}(\boldsymbol{Y}) + \mathfrak{h}(\boldsymbol{Y}|\boldsymbol{X}), \tag{17}$$

where $\mathfrak{h}$ is the entropy operator. Following the same approach as in [11], a closed form for I_{R} in (17) can be reached

$$I_{\mathrm{R}} = K + \log\big(\det(\boldsymbol{I}+\boldsymbol{G})\big) - \mathrm{Tr}\big(\boldsymbol{B}(\boldsymbol{I}+\boldsymbol{G})\big), \tag{18}$$

with the optimal $K \times K$ prefilter matrix $\boldsymbol{V}$ reads

$$\boldsymbol{V}_{\mathrm{opt}} = \left(\boldsymbol{H}\boldsymbol{H}^\dagger + \boldsymbol{I} \otimes \boldsymbol{R}\right)^{-1} \boldsymbol{H}\left(\boldsymbol{I}+\boldsymbol{G}\right), \tag{19}$$

[1]Under the case that $L-1$ zero-padding tail symbols are inserted between successive transmit blocks in order to eliminate interblock interference, the linear convolution is equivalent to the circular convolution.

where $\boldsymbol{B}$ is the mean square error matrix

$$\boldsymbol{B} = \left(\boldsymbol{H}^\dagger \left(\boldsymbol{I} \otimes \boldsymbol{R}^{-1}\right) \boldsymbol{H} + \boldsymbol{I}\right)^{-1}. \tag{20}$$

The operation $\boldsymbol{V}^\dagger \boldsymbol{Y}$ filters each diversity branch separately and the samples after filtering are summed up as

$$\hat{\boldsymbol{y}} = \boldsymbol{V}^\dagger \boldsymbol{Y} = \left(\sum_{n=0}^{N-1} \boldsymbol{v}_n * \boldsymbol{y}_n\right)^{\mathrm{T}}. \tag{21}$$

In (16), for the purpose of channel shortening, the matrix $\boldsymbol{G}$ is constrained to be a band-shaped Hermitian Toeplitz matrix with a memory length $\nu < L$, that is, only the middle $2\nu+1$ diagonals can take non-zero values. We define the first $\nu+1$ non-zero elements in the first column of $\boldsymbol{G}$ as

$$\boldsymbol{g} = [g_0 \ g_1 \ \cdots \ g_\nu].$$

Furthermore, $\boldsymbol{I}+\boldsymbol{G}$ is constrained to be positive definite [11] and we assume that

$$\boldsymbol{I} + \boldsymbol{G} = \boldsymbol{U}\boldsymbol{U}^\dagger, \tag{22}$$

where $\boldsymbol{U}$ is a $K \times K$ upper triangular Toeplitz matrix generated from the vector $\boldsymbol{u}$, which comprises the first $\nu+1$ non-zero elements in the first row of $\boldsymbol{U}$ as

$$\boldsymbol{u} = [u_0 \ u_1 \ \cdots \ u_\nu].$$

Denote $\check{\boldsymbol{u}} = [u_{\nu-1}^* \ \cdots \ u_0^*]$, and from (22) it holds that,

$$[g_\nu \ \cdots \ g_1 \ g_0 + 1 \ g_1^* \ \cdots \ g_\nu^*] = \boldsymbol{u} * \check{\boldsymbol{u}}. \tag{23}$$

The optimal $\boldsymbol{u}$ is designed to maximize I_{R} in (18), and the optimal prefilter $\boldsymbol{v}_n$ and coefficient $\boldsymbol{g}$ can be solved through (19) and (23), respectively. The algorithm is based on the DFT and inverse DFT (IDFT) operations and is summarized in Algorithm-1. The derivation is provided in Appendix A.

Algorithm-1: MILB channel shortening.

Input: Channel estimate $\hat{\boldsymbol{H}}$ and correlation matrix $\boldsymbol{R}$;

1. DFT of $\boldsymbol{h}_\ell$ for all diversity branches to obtain frequency response $\boldsymbol{\lambda}_k$ in eq. (27);
2. Calculate $\Delta_k = \left(\boldsymbol{\lambda}_k^\dagger \boldsymbol{R}^{-1} \boldsymbol{\lambda}_k + 1\right)^{-1}$ in eq. (28);
3. IDFT of Δ_k to obtain b_s, which are elements of MSE matrix $\boldsymbol{B}$ in eq. (29);
4. Calculate the optimal vector $\boldsymbol{u}$ based on b_s as in eq. (30) and eq. (31);
5. Calculate the optimal $\boldsymbol{g}$ based on eq. (23);
6. DFT of the optimal $\boldsymbol{u}$ to obtain U_m in eq. (32);
7. Calculate $\boldsymbol{\Theta}_s = \frac{|U_s|^2 \boldsymbol{R}^{-1} \boldsymbol{\lambda}_s}{1 + \boldsymbol{\lambda}_s^\dagger \boldsymbol{R}^{-1} \boldsymbol{\lambda}_s}$ in eq. (33);
8. IDFT of $\boldsymbol{\Theta}_s$ to obtain prefilters $\boldsymbol{v}_n$ in eq. (34);

Output: $\{\boldsymbol{v}_n\}_{n=0}^{N-1}$ and $\boldsymbol{g}$.

C. Complexity Analysis

It was shown in [13] that, computing the channel shortening prefilter coefficients in the MILB demodulator requires half the complexity as in the HOM demodulator. With diversity branches, the savings can also be achieved with Algorithm-1. This is because that, the inversion of covariance matrix $\boldsymbol{R}$ is required in both demodulators[2], and step 2 and 7 in Algorithm-1 require a low amount of scalar multiplications and inversions compared to the case with a single diversity branch in [13].

Next we evaluate the complexity of equalizers in the HOM and MILB demodulators, which is measured by the the number of real multiplications (one complex multiplication is counted as four real multiplications) per symbol stage. Notice that, the HOM demodulator requires a memory storage and updating process of the feedback symbols in all states with DDF-MLM equalizer. However, since the MILB channel shortener has truncated the channel tails, the MLM equalizer requires no feedback and is a simpler process than DDF-MLM equalizer.

Below we assume that the memory length in both equalizers is ν and the cardinality of the symbol modulation alphabet is $\mathcal{S}$. Then the number of states for both equalizers equals

$$N_{\#} = \mathcal{S}^{\nu}.$$

The branch metric calculation of the DDF-MLM equalizer in the HOM demodulator is based on the Forney model, and at the kth stage is calculated as

$$\gamma\left(x_k, \cdots, x_{k-\nu} | \hat{x}_{k-\nu-1}, \cdots, \hat{x}_{k-L+1}\right) \propto \sum_{n=0}^{N-1} \left| \hat{y}_k^n - \sum_{\ell=0}^{\nu} h_\ell^n x_{k-\ell} - \sum_{\ell=\nu+1}^{L-1} h_\ell^n \hat{x}_{k-\ell} \right|^2,$$

where $(x_k, \cdots, x_{k-\nu})$ are the symbols deduced from the current state, $\hat{y}_k^n$ is the filtered data obtained in (21), and $(\hat{x}_{k-\nu-1}, \cdots, \hat{x}_{k-L+1})$ are the feedback symbols on the survival path leading to the current state. Hence, it needs $N(4L+2)$ real multiplications to calculate γ. Since the branching factor is $\mathcal{S}$, the total complexity at each stage for the DDF-MLM equalizer is

$$C_{\mathrm{HOM}} = N(4L+2)N_{\#}\mathcal{S} = N(4L+2)\mathcal{S}^{\nu+1}. \tag{24}$$

On the other hand, the Ungerboeck model based branch metric of the MLM equalizer in the MILB demodulator is

$$\gamma(x_k, \cdots, x_{k-\nu}) \propto -2\mathcal{R}\left\{ x_k^* \left(\hat{y}_k^n - \sum_{\ell=1}^{\nu} g_\ell x_{k-\ell} \right) \right\} + g_0 |x_k|^2.$$

Since $g_0|x_k|^2$ is the same for all K stages, it can be pre-calculated[3] and the complexity of this part can be ignored. Hence, it needs $(4\nu+2)$ real multiplications to calculate γ. Since the branching factor is also $\mathcal{S}$, the total complexity at each process stage is

$$C_{\mathrm{MILB}} = (4\nu+2)N_{\#}\mathcal{S} = (4\nu+2)\mathcal{S}^{\nu+1}. \tag{25}$$

[2]In the HOM demodulator, the colored noise needs be whitened prior to the homomorphic filtering on each diversity branch.

[3]When x is modulated with a constant amplitude such as M-PSK, this term can be removed from the calculation.

To obtain low complexity, we set $\nu = 1$, and it holds that

$$\frac{C_{\mathrm{MILB}}}{C_{\mathrm{HOM}}} = \frac{(4\nu+2)\mathcal{S}^{\nu+1}}{N(4L+2)\mathcal{S}^{\nu+1}} = \frac{3}{N(2L+1)}.$$

For different modulations, the number of real multiplication is listed in Table 2 where we assume $N = 2$ and $L = 8$.

Table 2. Real Multiplication Number per Stage in Equalizer.

Modulation	S	$N_{\#}$	ν	C_{HOM}	C_{MILB}
GMSK	2	2	1	320	24
8PSK	8	8	1	5120	384
16QAM	16	16	1	20480	1536
32QAM	32	32	1	81920	6144

On the other hand, instead of computing $h_\ell^n x_{k-\ell}$ and $g_\ell^n x_{k-\ell}$ directly at each stage, when symbols x_ℓ utilize a fixed alphabet (which does not hold for GMSK modulation), they are the same for all K stages. Hence, they can be pre-calculated and stored. Then the branch metric calculation can use look-up-table (LUT) operations. With such an approach, the number of real multiplications required to calculate one branch metric is $N\mathcal{S}$ and $\mathcal{S}$ for the HOM and MILB demodulators, respectively. Therefore, C_{MILB} is still decreased by a factor of N over C_{HOM}. Meanwhile, the number of LUT operation in the MILB demodulator is only $(\nu+1)/L$ of the number of LUT operations in the HOM demodulator.

IV. NUMERICAL RESULTS

In this section we evaluate the performance of the proposed low-complexity two-stage receiver. The uncoded bit error rate (BER) and block error rate (BLER) are measured. We assume an E-EDGE system with a single transmit antenna and two receive antennas ($N = 2$). The uncoded BER and BLER are measured with different modulation and coding schemes (MCSs), and tested under typical urban (TU) and hilly terrain (HT) channels. The channel profiles are set according to the 3GPP specification [16]. We consider four different MCSs that are specified in Table 3 and $\nu = 1$ in all tests. In the plots, we denote the signal to noise power ratio as S/N and the signal to CCI power ratio as S/I, both in dB, respectively.

Table 3. MCS for E-EDGE Downlink [17].

MCS	Modulation	User Data Rate (kbps)	Coding Rate
MCS1	GMSK	8.8	0.53
MCS5	8PSK	22.4	0.37
MCS8	16QAM	54.4	0.67
MCS10	32QAM	67.2	0.65

In Figure 2 and Figure 3, we evaluate the CCI suppression performance for the MILB and HOM demodulators under TU channel at speed 3km/h. The S/N is fixed to 20dB and the performance without interference suppression is denoted with suffix 'NoIS'. As shown in Figure 2 and Figure 3, both the uncoded BER and BLER are significantly boosted by suppressing the CCI. At 10% uncoded BER, the gain with

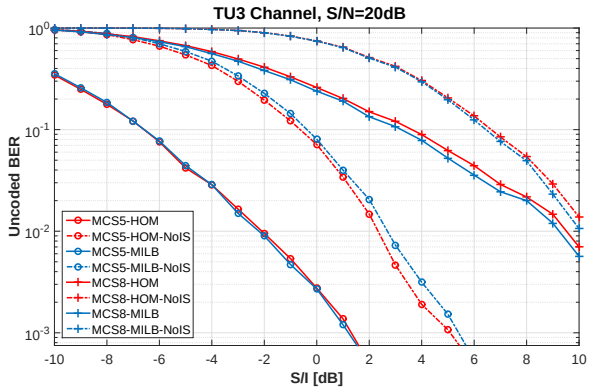

Fig. 2. Uncoded BER performance with TU3 channel.

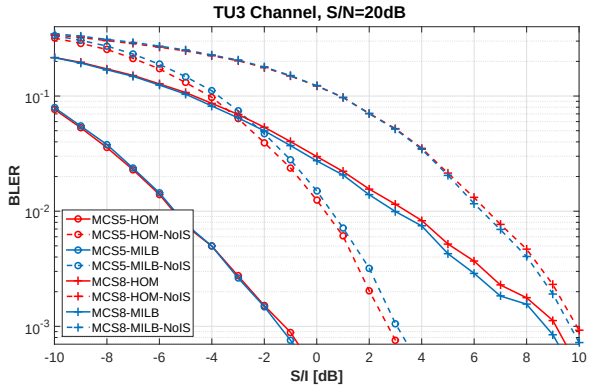

Fig. 3. BLER performance with TU3 channel.

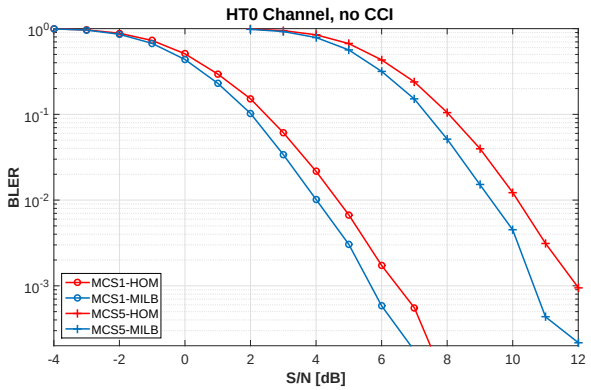

Fig. 5. BLER performance with HT0 channel.

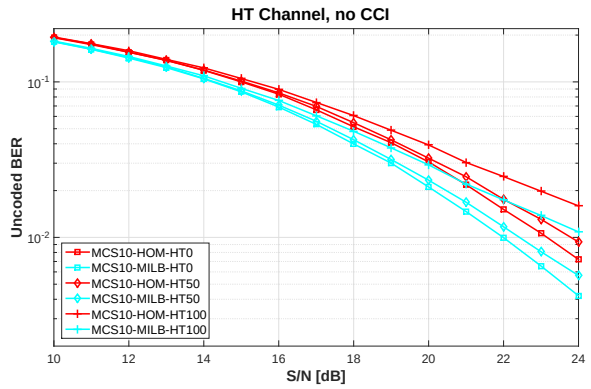

Fig. 6. Uncoded BER performance with HT0, 50 and 100 channels.

CCI suppression is around 6dB for MCS5 and 3dB for MCS8. The gain of MCS8 is reduced since, when S/I increases the interference level decreases, hence the impact of CCI suppression also degrades. As shown in Table 2, although the complexity of the MILB demodulator is much less than the HOM demodulator, with CCI suppressing the performance is almost the same with MCS5 as shown in both figures. With MCS8, the MILB demodulator shows a gain of about 0.2dB at 10% BLER above the HOM demodulator.

Next we test the cases without CCI and under HT channel, which has long tails and is difficult for channel shortening. As shown in Figure 4 and Figure 5, the MILB demodulator is superior to the HOM demodulator both with MCS1 and MCS5 under HT channel at no speed. With MCS10, as shown in Figure 6 and Figure 7, the MILB demodulator is around 1dB better at 10% uncoded BER and 2dB better at 1% BLER than the HOM demodulator at all speeds. Moreover, HT channel at 100 km/h is around 1dB worse than HT channel at no speed at 1% BLER.

V. Conclusions

In this paper we proposed a low complexity two-stage receiver with interference suppression and MILB channel shortening for single carrier SIMO systems. The first stage is CCI suppression, which removes the co-channel interference. In the second stage, the MILB channel shortener generates both the optimal prefilters and coefficient for the Ungerboeck model based MLM equalizer. The received samples from different diversity branches are summed up to a single data stream prior to the MLM equalizer. The proposed receiver is evaluated for an E-EDGE system. As shown by the numerical results, the first stage is very effective in suppressing the

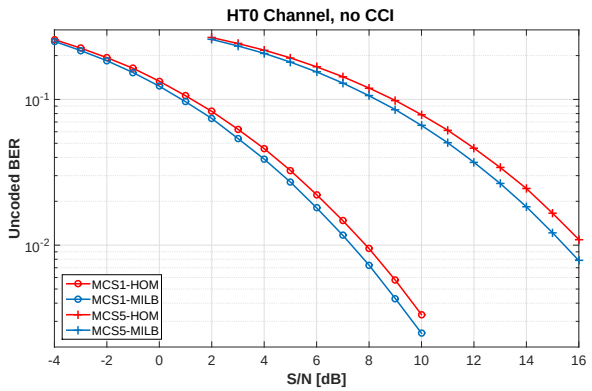

Fig. 4. Uncoded BER performance with HT0 channel.

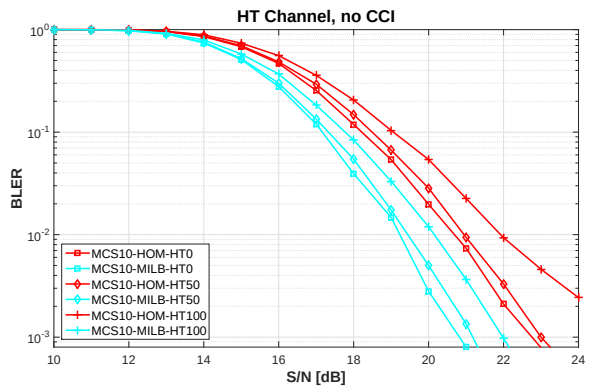

Fig. 7. BLER performance with HT0, 50 and 100 channels.

CCI. In the second stage, although the MILB demodulator truncates the channel tails and cooperates with a reduced-state MLM equalizer, it shows superior performance compared with the traditional homomorphic filter which cooperates with the DDF-MLM equalizer. Furthermore, the MILB channel shortening algorithm uses the discrete-Fourier transforms, which allows reusing resources from e.g. OFDM modems.

APPENDIX A

Denote the $K \times K$ Fourier matrix as $\boldsymbol{F}$ and the (s,n)th element as $F(s,n) = \exp(-2j\pi sn/K)$. The block circulant matrix $\boldsymbol{H}$ has the decomposition

$$\boldsymbol{H} = (\boldsymbol{F}^{-1} \otimes \boldsymbol{I})\boldsymbol{\Lambda}\boldsymbol{F}, \tag{26}$$

where $\boldsymbol{\Lambda} = \mathrm{diag}(\boldsymbol{\lambda}_0\ , \boldsymbol{\lambda}_1,\ \ldots\ , \boldsymbol{\lambda}_{K-1})$ is block diagonal and each block element $\boldsymbol{\lambda}_k = [\lambda_{k,0}\ \lambda_{k,1}\ \cdots\ \lambda_{k,N-1}]^{\mathrm{T}}$ is the $N \times 1$ column vector that comprises the DFT

$$\lambda_{k,n} = \sum_{\ell=0}^{L-1} h_\ell^n \exp\left(-\frac{2j\pi k\ell}{K}\right). \tag{27}$$

Inserting (26) back into (20), $\boldsymbol{B}$ can also be decomposed as

$$\boldsymbol{B} = \boldsymbol{F}^{-1}\boldsymbol{\Delta}\boldsymbol{F},$$

where the $K \times K$ diagonal matrix $\boldsymbol{\Delta}$ is

$$\boldsymbol{\Delta} = \left(\boldsymbol{\Lambda}^\dagger \left(\boldsymbol{I} \otimes \boldsymbol{R}^{-1}\right)\boldsymbol{\Lambda} + \boldsymbol{I}\right)^{-1},$$

and the kth diagonal element of $\boldsymbol{\Delta}$ reads

$$\Delta_k = \left(\boldsymbol{\lambda}_k^\dagger \boldsymbol{R}^{-1}\boldsymbol{\lambda}_k + 1\right)^{-1}. \tag{28}$$

Next we define the IDFT

$$b_s = \frac{1}{K}\sum_{k=0}^{K-1} \Delta_k \exp\left(\frac{2j\pi ks}{K}\right),\ 0 \le s < K. \tag{29}$$

By [11, Proposition 2], the optimal $\boldsymbol{U}$ that maximizes (18) is given by

$$u_0 = \frac{1}{\sqrt{b_0 - \boldsymbol{b}_\nu(\boldsymbol{B}_\nu)^{-1}\boldsymbol{b}_\nu^\dagger}}, \tag{30}$$

and

$$[u_1\ u_2\ \cdots\ u_\nu] = -u_0\boldsymbol{b}_\nu(\boldsymbol{B}_\nu)^{-1}, \tag{31}$$

where $\boldsymbol{b}_\nu$ is defined as

$$\boldsymbol{b}_\nu = [b_1^*\ b_2^*\ \cdots\ b_\nu^*].$$

and the $\nu \times \nu$ sub-matrix $\boldsymbol{B}_\nu$ of $\boldsymbol{B}$ is

$$\boldsymbol{B}_\nu = \begin{bmatrix} b_0 & b_1^* & \cdots & b_{\nu-1}^* \\ b_1 & b_0 & \cdots & b_{\nu-2}^* \\ \vdots & \vdots & \vdots & \vdots \\ b_{\nu-1} & b_{\nu-2} & \cdots & b_0 \end{bmatrix}.$$

Hence, the optimal vector $\boldsymbol{g}$ defined in (22) can be obtained through the optimal $\boldsymbol{u}$ as in (23). Defining the DFT

$$U_s = \sum_{k=0}^{\nu} u_k^* \exp\left(-\frac{2j\pi ks}{K}\right),\ 0 \le s < K, \tag{32}$$

and denoting $\boldsymbol{U}$ as the $K \times K$ diagonal matrix with U_m being its mth diagonal element, then the optimal $\boldsymbol{V}_{\mathrm{opt}}$ in (19) can be decomposed as

$$\boldsymbol{V}_{\mathrm{opt}} = \boldsymbol{F}^{-1}\boldsymbol{\Theta}(\boldsymbol{F} \otimes \boldsymbol{I}),$$

where the $K \times K$ block diagonal matrix $\boldsymbol{\Theta}$ is calculated by

$$\boldsymbol{\Theta} = \left(\boldsymbol{\Lambda}\boldsymbol{\Lambda}^\dagger + \boldsymbol{I} \otimes \boldsymbol{R}\right)^{-1}\boldsymbol{\Lambda}\boldsymbol{U}\boldsymbol{U}^\dagger,$$

and the mth block element $\boldsymbol{\Theta}_s = [\Theta_{s,0}\ \Theta_{s,1}\ \cdots\ \Theta_{s,N-1}]$ is an $N \times 1$ vector that can be calculated as

$$\boldsymbol{\Theta}_s = |U_s|^2\left(\boldsymbol{\lambda}_s\boldsymbol{\lambda}_s^\dagger + \boldsymbol{R}\right)^{-1}\boldsymbol{\lambda}_s = \frac{|U_s|^2\boldsymbol{R}^{-1}\boldsymbol{\lambda}_s}{1 + \boldsymbol{\lambda}_s^\dagger\boldsymbol{R}^{-1}\boldsymbol{\lambda}_s}. \tag{33}$$

Finally, the optimal filter $\boldsymbol{v}_n$ $(0 \le n < N)$ for nth diversity branch is obtained through the IDFT as

$$\boldsymbol{v}_n = \frac{1}{K}\sum_{s=0}^{K-1} \Theta_{s,n} \exp\left(\frac{2j\pi sn}{K}\right). \tag{34}$$

REFERENCES

[1] D. G. S. Kechiche and N. Jain, "From concept to delivery: The M2M market today," GSMA Intelligence, Feb., 2014.

[2] Ericsson, "GSM/EDGE optimization for Internet of Things," GP-140297, 3GPP TSG GERAN#62, May, 2014.

[3] H. Axelsson, P. Björkén, P. Bruin, S. Eriksson, and H. Persson, "GSM/EDGE continued evolution," Ericsson Review, no. 1, 2006.

[4] J. W. Liang, J. T. Chen, and A. J. Paulraj, "A Two-Stage hybrid approach for CCI/ISI reduction with SpaceTime processing," *IEEE Communications Letters*, vol. 1, no. 76, pp. 163-165, Nov., 1997.

[5] W. Koch amd A. Baier, "Optimum and sub-optimum detection of intersymbol interference," IEEE Global Telecommunications Conference (GLOCOM), vol. 3, pp. 1679-1984, Dec., 1990.

[6] G. D. Forney Jr., "Maximum likelihood sequence estimation of digital sequences in the presence of intersymbol interference," *IEEE Trans. on Inform. Theory*, vol. 18, no. 3, pp. 363-378, May, 1972.

[7] W. H. Gerstacker, F. Obernosterer, R. Meyer, and J. B. Huber, "On prefilter computation for reduced-state equalization," *IEEE Trans. on Wireless Communications*, vol. 1, no. 4, pp. 793800, Oct., 2002.

[8] C. Benkeser, S. Zwicky, H. Kröll, J. Widmer, and Q. Huang, "Efficient channel shortening for higher order modulation: Algorithm and architecture," *In Proc.* IEEE Int. Symp. Circuits Syst., pp. 2377-2380, May, 2012.

[9] H. Kröll, S. Zwicky, B. Weber, and C. Roth, "An evolved GSM/EDGE baseband ASIC supporting receive diversity," *IEEE Journal of Solid-State Circuits*, vol. 50, no. 7, pp. 1690-1701, Jul., 2015.

[10] A. Duel-Hallen and C. Heegard, "Delayed decision-feedback sequence estimation," *IEEE Trans. on Communications*, vol. 37, no. 5, pp. 428-436, May, 1989.

[11] F. Rusek and A. Prlja, "Optimal channel shortening of MIMO and ISI channels," *IEEE Trans. on Wireless Communications*, vol. 11, no. 2, pp. 810-818, Feb., 2012.

[12] F. Rusek, G. Colavolpe, and C. W. Sundberg, "40 Years with the Ungerboeck model: a look at its potentialities [lecture notes]," *IEEE Signal Process. Mag.*, vol. 32, no. 3, pp. 156-161, May, 2015.

[13] H. Kröll, S. Altorfer, T. Willi, A. Burg, and Q. Huang, "Channel Shortening and Equalization based on Information Rate Maximization for Evolved GSM/EDGE," IEEE Signal Processing Systems Workshop (SiPS), Oct., 2015.

[14] W. Hirt, *Capacity and information rates of discrete-time channels with memory*, Ph.D thesis, no. ETH 8671, Inst. Signal and Information Processing, Swiss Federal Inst. Technol., Zürich, 1988.
[15] U. Grenander anf G. Szegö, *Toeplitz forms and their applications*, University of Calif. Press Berkeley and Los Angeles, 1958.
[16] 3GPP TS 45.005, "Radio transmission and reception," Release 12.5.0, Mar., 2015.
[17] 3GPP TR 45.912, "Feasibility study for evolved GSM/EDGE radio access network (GERAN)," Release 12.0.0, Sep., 2015.